Geotechnical Aspects of Underground Construction in Soft Ground – Viggiani (ed)
© 2012 Taylor & Francis Group, London, ISBN 978-0-415-68367-8

Modelling a deep tunnel excavation in a low-porosity tectonised clay

D. Boldini
University of Bologna, Bologna, Italy

A. Graziani
University Roma Tre, Rome, Italy

ABSTRACT: The design of excavation in clayey soils is usually based on the hypothesis that the material displays undrained behaviour during construction. In the case of a deep tunnel, the high stress relief induced by excavation is associated to the development of a wide plastic zone where pore pressure may significantly decrease up to reach negative values in a wide area surrounding the tunnel walls. This type of hydro-mechanical behaviour, however, hardly applies to pervasively fissured scaly-clays, which can exhibit a macroscopic opening of fissures during stress release, resulting in a loss of saturation. In the paper, the stress-strain behaviour observed during construction of a large-diameter tunnel in scaly clays at depth as high as 400 m is reviewed. Different modelling approaches both for the short- and long-term conditions are investigated, ranging from a roughly simplified dry-medium model to a two-phase model with a coupling between permeability and plastic deformation.

1 INTRODUCTION

The hydro-mechanical behaviour of clayey soils and rocks can vary notably as a function of percentage and type of clay minerals, water content and possible presence of a fissure network, often caused by tectonic events.

In this respect, a useful classification is that proposed by the Comité Français de Méchanique des Roches (2000), which distinguishes between "plastic" and "rigid" clays:

- plastic, soil-like, clay formations generally are found at depths lower than 350 m and are characterised by a Young's modulus $E' < 500$ MPa and by a water content $w > 10\%$;
- stiff, rock-like, argillaceous formations (indicated with several geologic terms, such as marls, argillites, claystone, shales, argillaceous schist, etc.) are those characterised by a Young's modulus $E' > 2000$ MPa and by a water content $w < 10\%$.

This classification may also orientate the choice of the modelling approach. The main alternative, at least in the context of simple models suited to practical engineering applications, is between the "one-phase" and the "two-phases" approach. The first one, generally associated to visco-elastic or visco-plastic constitutive laws (e.g., Boidy *et al.* 2002, Boldini *et al.* 2004a, Debernardi & Barla 2009), is preferred for the stiff, rock-like, clays. The second one, in which time-dependent deformations are only due to consolidation phenomena (e.g., Gäber & Labiouse 2003, Carranza-Torres & Zhao 2009) is the classical approach for plastic clays. A combined approach (i.e viscous behaviour coupled to consolidation phenomena) was sometimes adopted (e.g., Bonini *et al.* 2009) although in this case greater difficulties arise in the estimation, at the field scale, of the many parameters which control hydro-mechanical and viscous behaviour.

This paper focuses on the response of "rigid" clays to tunnel excavation. Therefore, the discussed topics are mainly of interests for tunnelling in argillaceous rocks, such as argillites, mudstones and schist, frequently characterised by a scaly structure.

A common question the study should likely contribute to answer is: when is the rough hypothesis of "dry medium" actually acceptable for tunnel design in low-porosity argillaceous formations?

A further question is: which is the impact of the fissure network, on the hydro-mechanical response in the short- and long-term?

The influence of fissure opening as a consequence of the unloading process due to tunnel excavation is investigated in this paper by different phenomenological approaches which can be easily implemented in numerical Finite Element or Finite Difference models.

The proposed modelling approaches assume different limit behaviours of the plastic annulus around the tunnel, substantially controlled by the effect of fissure opening, which may cause loss of saturation, in the short-term, and a general increase in permeability, in the long-term.

The application of the proposed models will be discussed with reference to the case of the Raticosa tunnel, excavated in a scaly clay formation of central Italy (Boldini *et al.* 2004b).

2 MODELLING APPROACHES

Static analysis of geotechnical structures in low-permeability grounds is frequently carried out for two idealised situations: the short-term conditions ($t = 0$), characterised by the undrained behaviour of the porous medium, and the long-term conditions ($t = \infty$), in which a stationary pore pressure distribution is reached.

In Appendix, some useful analytical solutions for the two aforementioned limit conditions are summarised.

The excess pore pressures Δp generated by tunnel excavation and the new boundary conditions imposed at the tunnel wall (i.e., by a pervious or impervious lining) initiate a time-dependent groundwater flow until the final stationary pore pressure distribution is established. During the transitory phase (consolidation process) an increase in the loading applied on the lining generally occurs.

For tunnelling in clay formations, it is routinely assumed that ideal undrained conditions hold during the excavation stages. However, the interaction between pore water and soil skeleton exhibits unconventional features in fissured or tectonised formations of very low porosity (Gasc-Barbier *et al.* 1999), where the available free water can be rather limited and fissure opening due to stress relief favours desaturation.

In the following, specific modelling approaches are presented in order to appreciate the influence of fracture opening. The mechanical behaviour of the ground is simply modelled as an ideal elasto-plastic medium, characterised by the Mohr-Coulomb strength criterion.

Four different hypotheses were formulated in order to evaluate the hydro-mechanical response in the short-term (Fig. 1):

- Model 1: conventional undrained behaviour;
- Model 2: undrained behaviour with tensile strength of water equal to zero;
- Model 3: undrained behaviour with pore pressure set equal to zero in ground zones as plastic deformation develops;
- Model 4: dry-medium behaviour.

Model 1 and Model 4 can be seen as two limit behaviours, which encompass the real hydro-mechanical response during tunnel excavation.

Model 3 assumes that the pore pressure suddenly drops to zero in the elasto-plastic region due to the opening of fissures during unloading.

For the long-term situations two possible hypotheses were considered. The first assumes that plastic deformations do not change permeability inside the plastic annulus around the tunnel (i.e., $k_{el} = k_{pl}$). In the calculations, this hypothesis was associated to short-term Models 1, 2 and 4. The second assumption represents the limit case of a plastic annulus characterised by infinite permeability with respect to the undisturbed ground in the elastic zone, as a consequence of fissure opening (i.e., $k_{el}/k_{pl} = 0$). It was associated to Model 3.

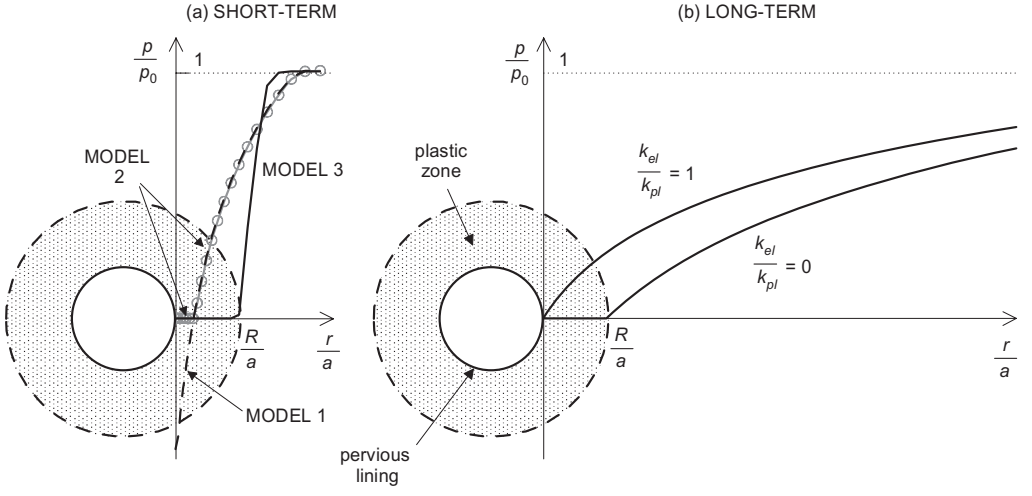

Figure 1. Possible schemes of pore-pressure distribution for short- (a) and long-term situation (b). a is the tunnel radius, R the plastic radius and p_0 the undisturbed in situ pore pressure.

3 RATICOSA TUNNEL

The Raticosa tunnel is one of the several tunnels realised for the new Bologna-Florence high-speed railway line (Italy). The tunnel, having an overburden of up to 500 m, is located in the Apennine chain and crosses a tectonized clay-shale formation called Chaotic Complex for about 4.5 km (Fig. 2).

The chaotic structure of such formation is the result of tectonic actions from Miocene-Pliocene to Plio-Pleistocene. The Chaotic Complex is mainly composed by a pelitic matrix with dispersed and disaggregated lithic components. The matrix is formed by an assemblage of clay scales of the size of millimetres to centimetres whose surfaces are curved, smooth and at times striated. Mineral composition, obtained by X-ray diffraction, was found to be very variable. Deeper samples are characterised by a lower phyllo-sillicate content (25%–30%), which increases to 40%–50% for the shallower samples. Smectite is generally present in small proportion in the form of alternating illite-smectite layers.

The tunnel (diameter D = 14 m) was full-face excavated with an hydraulic hammer. Due to the poor mechanical properties and to the expected heavy squeezing conditions, full face-excavation required face reinforcement using fibre-glass dowels (35–80 dowels, 20–24 m in length, installed every 10–12 m of tunnel advance). A closed-ring primary lining, consisting of a shotcrete layer (thickness 0.25–0.30 m) and steel sets (2 IPN220 including an arched strut in the invert), was applied at each round of excavation (length 1.0–1.2 m). The final lining, made of reinforced concrete (invert and sidewalls) and plain concrete (vault), was completed at a maximum distance from the face of 2D.

3.1 *Laboratory testing*

The clayey formation is characterised by a very low natural water content and can be identified, according to the classification of the Comité Français de Méchanique des Roches (2000), as a stiff, indurated clay.

A summary of the physical and index properties (Boldini *et al.* 2004b) measured on specimen and block samples taken at depths ranging from 175 and 520 m is given in Table 1, although it should be reminded that the geotechnical characterisation of structurally complex formations presents many uncertainties.

An indirect indication of the tendency to dilation and loosening during unloading of the scaly structure of such formation is provided by the value of saturation degree measured in laboratory specimen, generally appreciably lower than unity (Table 1).

Figure 3 shows the results of one-dimensional Huder-Amberg test obtained for a sample trimmed from a block recovered from the tunnel face at a depth of 430 m. The test procedure is similar to the conventional oedometer compression test, the only difference being that the first loading, unloading and reloading stages are performed without adding water in the apparatus. The first loading-unloading cycle (point C) seems sufficient to recover an approximately undisturbed initial state, characterised by high saturation degrees and, possibly, closed fissures.

Table 1. Index and physical properties of the tectonised clays at a depth ranging from 175 to 520 m (Boldini *et al.* 2004b).

Unit weight of total volume γ (kN/m^3)	20.8–24.1
Unit weight of solid γ_s (kN/m^3)	26.7–27.3
Natural water content w (%)	2.4–9.4
Liquid limit w_L (%)	30–41
Plastic limit w_P (%)	16–20
Saturation degree S_r (%)	48–94
Clay fraction (%)	3–20
Permeability k (m/s)	$<10^{-11}$

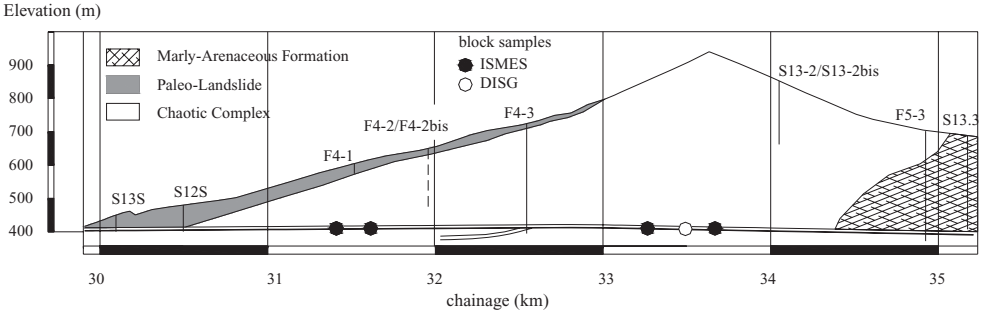

Figure 2. Geological profile along the Raticosa tunnel (Boldini et al. 2004b).

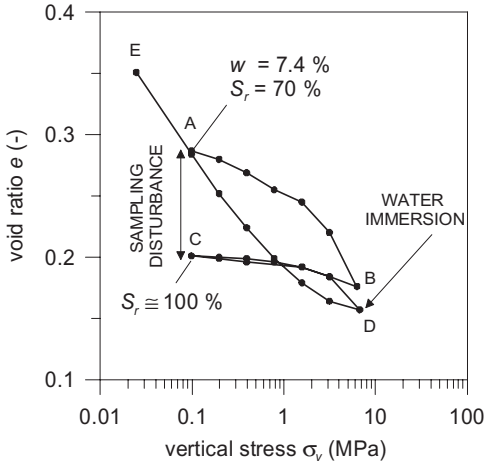

Figure 3. Results of a Huder-Amberg test performed on a sample taken at the tunnel face at the depth of 430 m (Boldini *et al.* 2004b).

Swelling after water immersion (point D) was negligible, thus, it can be argued that the swelling pressure is lower than the applied stress $\sigma_{v,D}$, which in turn was set approximately equal to the vertical lithostatic stress at the sample depth, under the assumption of pore pressure $p_0 = 0$ (hypothesis of dry-medium). On the base of the previous experimental results, the hypothesis of fully saturation and hydrostatic pore pressure distribution cannot be rejected. Therefore, it represents one of the possible scenarios considered in the following numerical investigations.

3.2 *Monitoring data*

At present, no reliable information is available on water table position and pore pressure distribution inside the Chaotic Complex. 14 vibrating wire piezometres, installed during tunnel excavation up to a distance of 15 m from the tunnel wall, have not given so far significant measurements of pore pressure. This evidence can be reasonably explained as an effect of the scaly structure of the formation, characterised by fissures that can be easily sheared and opened by the unloading caused by tunnel excavation.

The whole construction process was performed under the continuous control of a monitoring system, mainly based on the geodetic survey of tunnel wall displacements ("convergence" measurements) and on deformation measurements carried out by a sliding micrometer along pipes installed from the face in the direction of the tunnel axis ("extrusion" measurements).

In this study, attention was focused only on convergence measurements since they can be easily compared with the displacements of the tunnel cross-section predicted by plane strain models.

Figure 4 shows two examples of convergence measurements along the horizontal diameter as a function of the distance x of the monitoring section from the tunnel face. These data refer to monitoring sections at depths ranging from 325 to 375 m.

The convergence measurements were interpolated by empirical laws in order to evaluate separately evaluating the two contributions of face advance and time.

The "instantaneous" diametric convergence of the tunnel at great distance from the face, C_∞, which also includes the displacement C_0 occurred before the zero reading, is obtained by the well-known relationship of Panet & Guenot (1982):

$$C(x) = C_f + \left(C_\infty - C_f\right)\left[1 - \left(\frac{0.84R}{x + 0.84R}\right)^2\right] \qquad (1)$$

where C_f is the convergence of the diameter at the face and R is the plastic radius (Fig. 1). For an elastic medium, C_f is equal to $0.27 \cdot C_\infty$ but the same relationship approximately holds also for an elasto-plastic medium, if C_∞ is properly evaluated.

Data fitting was performed by adopting the procedure described in Graziani *et al.* (2005) which consists in assuming relationship (1) as a shape function and in estimating the section-specific C_∞ value on the basis of the first two measurements of convergence. Adopting a plastic radius R equal to twice the tunnel radius, the estimated total horizontal convergence resulted to be within the interval 0.06–0.18 m for all the available monitoring sections at depths ranging from 325 to 375 m.

Most of the monitoring sections exhibit some amount of time-dependent deformations, as demonstrated by convergence measurements that go on increasing even after the face effect is exhausted (practically, for $x > 2a$, having indicated with a the tunnel radius, and time $t > 7$ days) (Fig. 5).

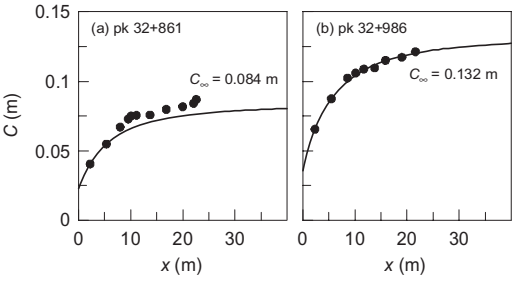

Figure 4. Measured diametric convergences versus face distance and their interpolation by Panet & Gunet (1982) empirical law.

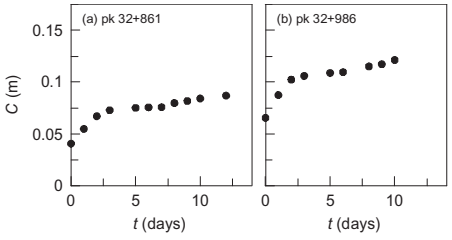

Figure 5. Measured diametric convergences versus time.

4 NUMERICAL MODEL

The numerical model considers a circular tunnel (radius $a = 7$ m) at a depth of 350 m, assuming an isotropic state of initial stress ($S_0 = 8.05$ MPa at the depth of the tunnel axis). The mechanical parameters required for the assumed ideal elasto-plastic model are: Young's modulus $E' = 2000$ MPa, Poisson's ratio $\nu' = 0.3$, cohesion $c' = 200$ kPa, friction angle $\varphi' = 15°$; the dilatancy angle ψ is 0° or 5°.

Plane-strain numerical analyses were performed by the finite difference code FLAC (ITASCA 2005), adopting a coupled solution scheme. A fully axisymmetric model, which implies that gravity is disregarded, was preferred in order to make the numerical model as much as possible comparable to the analytical solutions. The grid represents a quarter of tunnel, with the interval (a, r_{max}) of the calculation domain subdivided into 60 elements (Fig. 6). At the external boundary ($r_{max} = 20\ a$) stress conditions corresponding to the lithostatic situation were applied.

The main differences between the analytical and numerical approaches stem from the limited extent of the grid (r_{max}) and the imposed boundary conditions for $r = r_{max}$.

The analysis of data from the monitoring sections indicates a radial convergence (i.e., half of the diametric convergence C) of the tunnel before support installation in the range 20–30 mm and a total measured increment of radial convergence approximately equal to 30 mm.

Values of convergences in agreement with such measurements can be obtained in the numerical models by assuming a relaxation factor $\lambda = 0.5$ at the time of support activation (general reference about the definition and use of the relaxation factor can be found, e.g., in Panet & Guenot 1982). More precisely, the relief ($\lambda = 0.5$) was calibrated with reference to the case of Model 3, which can be considered the most realistic, as discussed in the following.

The same stress relief is used in Figure 7 to find the starting point of the support curve when applying the Characteristic Curves method.

Considering the short-term characteristic curve of the tunnel represented in Figure 7, the 30 mm increment in convergence undergone by the support is compatible with an overall stiffness of the support system $K_l = \Delta q/\Delta u_a = 100$ MPa/m. Again, this back-calculated stiffness corresponds to an equivalent Young's modulus of 16 GPa, for a lining thickness of 0.3 m, as assumed for the beam elements utilised to model the lining.

The effect of face reinforcement was not considered in the model, but its potential influence on wall convergence arises implicitly from the calibration of the stress relief by the monitoring data.

Figure 7 also shows the long-term characteristic curve for the perfectly pervious tunnel, calculated by the analytical solution (Eq. (A7) reported in Appendix).

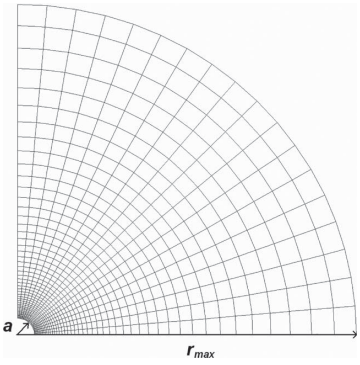

Figure 6. Mesh employed in the numerical analyses.

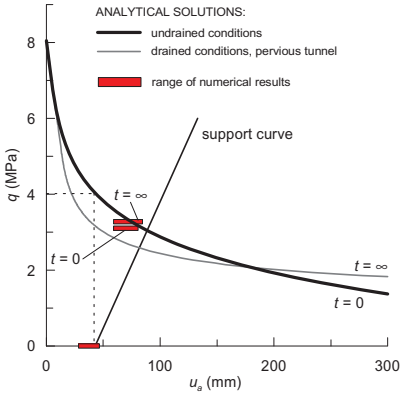

Figure 7. Characteristic curves for the tunnel in drained and undrained conditions and for the lining; the range of numerical results for different models is also indicated.

5 RESULTS

The distribution of pore pressure obtained by the different modelling approaches are reported

in Figure 8a, which refers to the short-term equilibrium conditions after lining installation. The conventional undrained analysis with a small dilatancy angle (Model 1b, $\psi = 5°$) is the only case in which negative pore pressures develop around the tunnel. Looking at the pore pressure profiles, the limit of the plastic zone can be identified as the point where pore pressure starts to decrease from the undisturbed value p_0. It can be noticed that the extent of the plastic zone is smaller for Model 3, in which pore pressure is set equal to zero as soon as plastic strains develop.

Figure 8b shows the long-term profiles of pore pressure, according to the two possible idealised steady-state situations, previously defined. The striking difference between the two pore pressure profiles can be roughly viewed as a "shift" of the curve from the tunnel wall to the limit of the plastic annulus.

Figure 9 illustrates the increment in displacement for three characteristic phases of tunnel life, namely, before and after lining installation, in the short-term, and at the end of the consolidation process.

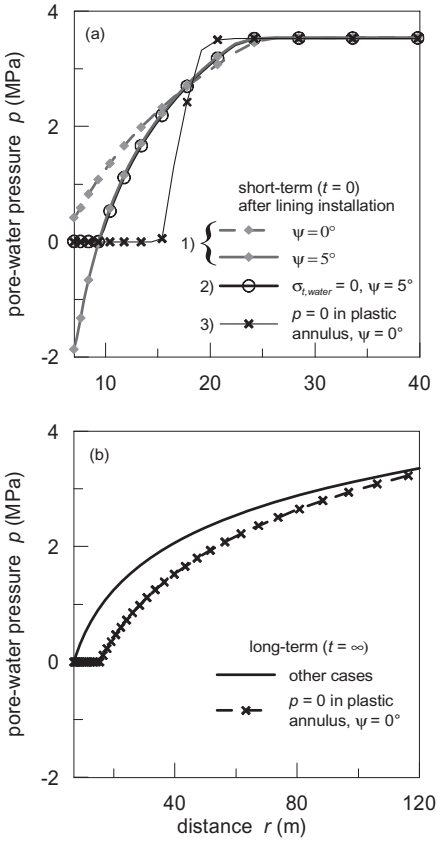

Figure 8. Pore-pressure distribution around the tunnel in the short- (a) and long-term (b), for Model 1, 2 and 3.

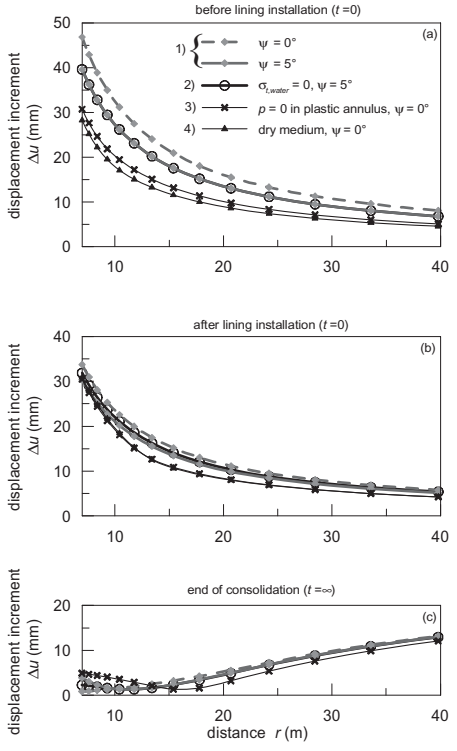

Figure 9. Distribution of displacement increment around the tunnel occurred before (a) and after the lining installation (b) and at the end of the consolidation process (c).

The increment in tunnel convergence before lining installation (Fig. 9a) is significantly different for the various models: maximum and minimum values are obtained for the conventional undrained analysis (Model 1) and the dry medium analysis (Model 4), respectively. A modest dilatancy angle (Model 1b) tends to reduce the displacement. Moreover, Model 1b and Model 2 give the same results, indicating that negative pore pressures are not yet present, while they develop due to the second phase of stress relief, i.e., after placement of the lining (Fig. 9b).

The different ways of modelling solid-water interaction, in the short-term, seem to have a negligible influence on the increase in displacement after lining installation (Fig. 9b), and consequently on the support load. At this stage, the calculated total diametric convergence varies between 120 and 150 mm, thus resulting slightly larger than the "instantaneous" closure obtained from monitoring data.

The displacement increments due to consolidation predicted by the different models are comparable far from the tunnel wall, while, although being modest, differ significantly near the excavation

(Fig. 9c). The calculated increment in radial convergence ranges between 1 and 5 mm. This means that the ratio between the time-dependent closure and the "instantaneous" closure is less than 10%, a value significantly lower than those obtained from the regression analysis of monitoring data (around 27%). It can be therefore argued that most of time-dependent deformation is of viscous nature and, therefore, that pore pressure equalization plays a minor role.

Finally, a comparison in terms of convergence and lining load between the various numerical predictions and the analytical characteristic curves is shown in Figure 7, for the three main steps of calculation (i.e., before lining installation, after lining installation in the short-term and at the end of the consolidation process). The long-term analytical (i.e., uncoupled) solution gives erroneous predictions, as generally occurs for the case of pervious lining (Graziani & Ribacchi 2001).

6 CONCLUSIONS

The paper analyses specific issues concerning the hydro-mechanical response of fissured argillaceous rocks to tunnelling. The study started from the case-history of a deep tunnel excavated in a highly tectonized clay formation (Raticosa tunnel, Italy). A common problem in this kind of structurally-complex formations is the difficulty in obtaining reliable measurements of pore pressure and, thus, the uncertainty in formulating the most appropriate model of solid skeleton-pore water interaction.

A wide range of conceptual models for the short-term behaviour were compared, ranging from the conventional undrained response to models specifically formulated for stiff fissured clays, for which the development of negative pore pressure during unloading stress paths may be limited as a consequence of shearing and opening of fissures. The limit case of a fully dry medium was also considered.

For the long-term situation, two idealised cases were considered, depending of the permeability of the plastic annulus around the tunnel, which can be assumed either equal to that of the undisturbed ground or infinite, again as a consequence of fissure opening.

It was found that the different models predict significantly different convergences of the tunnel wall in the situation before lining installation, but have only a modest influence on support loads. Even the simplest model of fully dry-medium could provide a satisfactory estimate of the short- and long-term load on the lining.

Since the proposed models encompass a very wide range of possible hydro-mechanical responses, they could represent an useful tool to asses the impact of uncertainties about the real behaviour of complex geo-materials, particularly in the preliminary design of deep tunnels.

For the case of Raticosa tunnel, increment in tunnel closure due to consolidation processes, as predicted by the proposed models, represent only a part of the measured time-dependent increment. Most of the delayed convergence seems to be caused by viscous deformation of the rock.

7 APPENDIX

All the analytical solutions herein considered refer to a cylindrical borehole in an infinite medium.

7.1 *Short-term conditions*

A simple analytical solution (Salençon 1959) for the undrained situation is based on the following hypotheses: circular tunnel of radius a, ideal elasto-plastic medium and axisymmetry conditions with isotropic in situ total stress S_0 and uniform pore water pressure p_0.

The undrained behaviour of the porous medium is obtained by considering a null volumetric deformation and a purely cohesive shear strength, equal to c_u. The plastic radius R (distance of the outer boundary of the plastic zone from the tunnel axis) and the radial displacement u are given by the following expressions:

$$\frac{R}{a} = \exp\frac{\mathrm{OF}-1}{2} \quad \text{with} \quad \mathrm{OF} = \frac{S_0 - q}{c_u} \tag{A1}$$

$$\frac{u(r)}{a} = u_a \cdot \frac{1}{r} = \frac{c_u}{2G}\exp(\mathrm{OF}-1)\cdot\frac{a}{r} \tag{A2}$$

G is the shear elastic modulus, q the tunnel support pressure and, OF the so called Overload Factor.

In the plastic annulus around the tunnel, σ_r and σ_θ, the total radial and the circumferential stress, are obtained by equilibrium and plasticity conditions:

$$\sigma_r = q + 2c_u \ln\frac{r}{a} \qquad \sigma_\theta = q + 2c_u\left(1 + \ln\frac{r}{a}\right) \tag{A3a,b}$$

The excess pore pressure Δp must be equal to the variation of the total mean stress; hence, the distribution of Δp around the opening is given by:

$$\Delta p = p - p_0 = -S_0 + q + c_u\left(1 + 2\ln\frac{r}{a}\right) \text{ for } r \le R$$
$$\Delta p = 0 \text{ for } r > R \tag{A4}$$

Finally, given all the aforementioned hypotheses, the undrained cohesion c_u can be expressed as a

function of the drained strength parameters c_u, c', φ':

$$c_u = (S_0 - p_0)\ \sin\varphi' + c'\cos\varphi' \qquad \text{(A5)}$$

7.2 *Long-term conditions*

Regarding the long-term conditions ($t = \infty$), Lembo-Fazio and Ribacchi (1984) proposed to evaluate the state of stress and deformation around deep tunnels assuming that a stationary radial flow establishes inside an annular zone spanning from the tunnel wall to a radius r_0, which represents the limit of the zone influenced by seepage (i.e., $p = p_0$ for $r \geq r_0$). The corresponding pore pressure distribution is:

$$p(r) = p_a + (p_0 - p_a)\ \ln\left(\frac{r}{a}\right) \Big/ \ln\left(\frac{r_0}{a}\right) \qquad \text{(A6)}$$

where p_a is the value of pore pressure at the tunnel wall.

The general solution for stresses and displacements around the tunnel is described in Lembo-Fazio and Ribacchi (1984); afterward, it was applied by Graziani and Ribacchi (2001) to the case of uncompressible fluid and elasto-plastic solid skeleton. For an ideal plastic medium with a Mohr-Coulomb strength criterion (cohesion c', friction angle φ', dilation angle ψ'), it is given by Eq. (A7).

p_R is the value of pore water pressure at the plastic radius R; G and ν' are the usual elastic constants; h is a parameter which takes the influence of the pore pressure gradient into account; N and K are, respectively, the triaxial and dilatancy factors.

$$\begin{aligned}\frac{u}{a}\cdot 2G = &\left[(S_0 - p_0)\sin\varphi' + (p_0 - p_R)\frac{1-2\nu'+\sin\varphi'}{2(1-\nu')}\right]\frac{(R/a)^{K+1}}{(r/a)^K} \\ &+\left[(S_0 - p_0 + c'\cdot\cot g\varphi')(1-2\nu') - h\frac{1+NK-\nu'(K+1)(N+1)}{K+1}\right] \\ &\cdot\left[\frac{(R/a)^{K+1}}{(r/a)^K} - (r/a)\right] + \\ &-\left[\frac{(q - p_0 + c'\cdot\cot g\varphi' - h)}{\dfrac{1+NK-\nu'(K+1)(N+1)}{K+1}}\right] \\ &\cdot\left[\frac{(R/a)^{K+1}}{(r/a)^K} - (r/a)^N\right]\end{aligned} \qquad \text{(A7)}$$

$$\frac{R}{a} = \left\{\frac{(1-\sin\varphi')\cdot\left[S_0 - p_R - \dfrac{(1-2\nu')}{2(1-\nu')}\times(p_0 - p_R)\right] + c'\cdot\cot g\varphi' - h}{q - p_a + c'\cdot\cot g\varphi' - h}\right\}^{\frac{1}{N-1}} \qquad \text{(A8)}$$

$$h = \frac{p_0 - p_a}{(N-1)\cdot\ln(r_0/a)}, \quad N = \frac{1+\sin\varphi'}{1-\sin\varphi'}, \quad K = \frac{1+\sin\psi'}{1-\sin\psi'} \qquad \text{(A9a,b,c)}$$

REFERENCES

Boidy, E., Bouvard, A. & Pellet, F. 2002. Back analysis of time-dependent behaviour of a test gallery in claystone. *Tunn. Undergr. Sp. Tech.* 17: 415–424.

Boldini, D., Lackner, R. & Mang, H.A. 2004a. Influence of face reinforcement and shotcrete support on static conditions of deep tunnels: a thermo-chemo-mechanical study. *Rivista Italiana di Geotecnica* 4: 52–69.

Boldini, D., Graziani, A. & Ribacchi, R. 2004b. Raticosa tunnel, Italy: characterization of tectonized clay-shale and analysis of monitoring data and face stability. *Soils and Foundations* 44: 59–71.

Bonini, M., Debernardi, D., Barla, M. & Barla, G. 2009. The mechanical behaviour of clay shales and implications on the design of tunnels. *Rock Mech. Rock. Engng*. 42(2): 361–388.

Carranza-Torres, C. & Zhao, J. 2009. Analytical and numerical study of the effect of water pressure on the mechanical response of cylindrical lined tunnels in elastic and elasto-plastic porous media. *Int. J. Rock Mech. Min. Sci.* 46: 531–547.

Comité Français de Méchanique des Roches 2000. *Manuel de méchanique des roches. Tome 1: Fondaments. Roches Argileuses.* Paris: Les Presses de l'Ecole des Mines.

Debernardi, D. & Barla, G. 2009. New viscoplastic model for design analysis of tunnels in squeezing conditions. *Rock Mech. Rock. Engng.* 42(2): 259–288.

Gasc-Barbier, M., Ghoreychi, M. & Tessier, D. 1999. Comportament mécanique de roches argileuses profondes: incidence de la texture. *Proc. 9th ISRM Congr., Paris*, 595–600.

Gäber, R. & Labiouse, V. 2003. Influence of pore water on the design of deep galleries in low permeability rocks. *Proc., 10th ISRM Congr., Johannesburg*, 347–350.

Graziani, A., Boldini, D. & Ribacchi, R. 2005. Practical estimate of deformations, loads and stress relief factors for deep tunnel supported by shotcrete. *Rock Mechanics and Rock Engineering* 38: 345–372.

Graziani, A. & Ribacchi, R. 2001. Short- and long-term load conditions for tunnels in low permeability ground in the framework of the convergence-confinement method. *Proc. Intern. Symp., Kyoto,* 83–88.

ITASCA 2005. *FLAC, User's Manual, Version 5.0*. Itasca Consulting Group Inc., Minneapolis, Minnesota.

Lembo-Fazio, A. & Ribacchi, R. 1984. Influence of seepage on tunnel stability. *Proc., Int. Conf. on Design and Performance of Underground Excavations, Cambridge*, 173–181.

Panet, M. & Guenot, A. 1982. Analysis of convergence behind the face of a tunnel. *Proc., Tunneling 82, Brighton*, 197–204.

Salençon, J. 1969. Contraction quasi-statique d'une cavité à symétrie sphérique ou cylindrique dans un milieu éleastoplastique. *Ann. Ponts et Chaussées* 4: 231–236.